

SUPPLEMENTARY INFORMATION

- Observation of Bogoliubov excitations in exciton-polariton condensates -

We describe here the underlying theory and experiment for the observation of Bogoliubov excitations in exciton-polariton condensates, focusing on the theoretical analysis based on the Gross-Pitaevskii (GP) equation. The nonlinear characteristics of the condensate energy ε_0 , the position uncertainty Δx and the momentum uncertainty Δk are numerically evaluated as a function of the polariton number n or the pump rate P/P_{th} . We will analyze the excitation spectra of the trapped condensates taking into accounts the spatial inhomogeneity of the experimental systems. We will also discuss the contribution of thermal depletion and quantum depletion in the observed excitation spectrum.

I. THE GROUND STATE OF A CONDENSATE

For weakly interacting bosons in a dilute limit (14), a single particle field $\Psi_0(\vec{r})e^{-i\frac{\varepsilon_0}{\hbar}t}$ can be introduced to describe the wave function of the condensate ground state,

$$\Psi_0(\vec{r}) = \prod_{I=1}^{N_0} \Psi_0(\vec{r}_I)$$

where \vec{r}_I is the coordinate of the I -th particle in the two dimensional system and N_0 is the number of particles in the ground state.. At a temperature well below the critical temperature of condensation, $\Psi_0(\vec{r})$ obeys the following non-linear Schoedinger equation (or Gross-Pitaevskii equation):

$$\left(-\frac{\hbar^2}{2m}\nabla^2 + V(\vec{r}) \right) \Psi_0(\vec{r}) + g|\Psi_0(\vec{r})|^2\Psi_0(\vec{r}) = \varepsilon_0\Psi_0(\vec{r}) \quad (1)$$

where $V(\vec{r})$ is an external potential for the particles and ε_0 is the ground state energy per particle of the condensate. The non-linear term in this equation results from the interaction between the particles with an interaction energy $g \equiv \frac{U(n')}{n'}$, where $U(n')$ is a density dependent interaction energy introduced in the main text and a contact interaction with the form $\int d\vec{r}_1 d\vec{r}_2 g \delta(\vec{r}_1 - \vec{r}_2) \Psi^\dagger(\vec{r}_1) \Psi^\dagger(\vec{r}_2) \Psi(\vec{r}_2) \Psi(\vec{r}_1)$ has been assumed. (Please note that g is not an exciton-polariton splitting in this section.) Here n' is the local density of the condensate. The state $\Psi_0(\vec{r})$ describes the local condensate density as $n'(\vec{r}) = |\Psi_0(\vec{r})|^2$ and is renormalized to the total number of condensate particles as $\int d\vec{r} |\Psi_0(\vec{r})|^2 = n$. For a homogeneous system, the solution of Eq. (1) is approximated by $\Psi_0 = \sqrt{n'}$ with $n' = n/S$ and S is the size of the condensate, and $\varepsilon_0 = U(n') = gn'$.

For the exciton-polaritons in a microcavity, the system is not homogeneous either because of the Gaussian profile of the pumping laser beam or because of an external trapping potential. The effect of the Gaussian profile on the condensate has been thoroughly studied in our previous publication (4,26). First, we focus on the property of the condensate in an external trapping potential. In our system, a metallic layer provides a small cylindrical trapping potential of $V_0 \simeq 200\mu eV$ for the exciton-polaritons inside a trap of radii $R_0 = 3.5 - 4 \mu m$. Meanwhile, it also reduces the absorbed pump power by $\sim 50\%$ for the area under the metallic layer.

We consider the solution of Eq. (1) in a two-dimensional system with the cylindrical coordinates (r, θ) . The ground state wave function can be written as $\Psi_0(r) = \frac{\phi_0(r)}{\sqrt{r}}$ and $\phi_0(r)$ obeys the equation

$$\left\{ -\frac{\hbar^2}{2m} \left[\frac{\partial^2}{\partial r^2} + \frac{1}{4r^2} \right] + V(r) \right\} \phi_0(r) + g \frac{\phi_0^3(r)}{r} = \varepsilon_0 \phi_0(r) \quad (2)$$

which can be solved numerically with the steepest descent method (14). For non-interacting particles, the solution

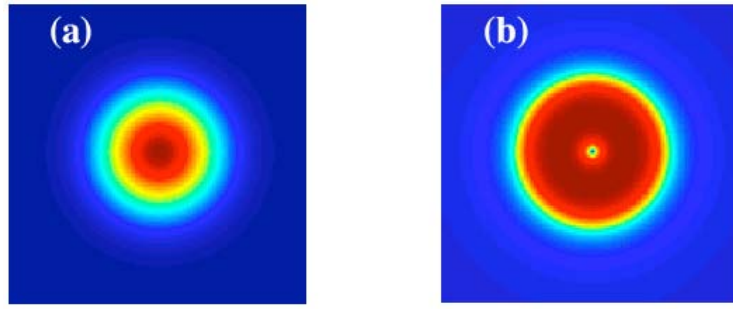


FIG. 1: Condensate density for the exciton-polaritons. (a) Condensate density for non-interacting polaritons. (b) Condensate density for interacting polaritons with $n = 3 \times 10^5$ and $P/P_{th} = 5$.

of Eq. (2) is given by the Bessel functions as

$$\phi_0(r) = \begin{cases} c_i J_0(k_0 r), & r \leq R_0 \\ c_e K_0(k'_0 r), & r > R_0 \end{cases}$$

with $k_0 = \sqrt{2m(V_0 + e_0)/\hbar^2}$, $k'_0 = \sqrt{2m(-e_0)/\hbar^2}$ and $e_0 (< 0)$ being the ground state energy without interaction. Here, $c_{i,e}$ are the normalization coefficients determined by the boundary conditions. With $m = 10^{-4}m_e$, where m_e is the bare electron mass, we derive that $e_0 = -0.11 \text{ meV}$ for $R_0 = 3.5 \mu\text{m}$ and $V_0 = 200 \mu\text{eV}$. The standard deviation of the ground state in coordinate space is $\Delta x = 1.86 \mu\text{m}$ and the deviation in momentum space is $\Delta k = 0.28(\mu\text{m})^{-1}$, with $\Delta x \Delta k \sim 0.52$ close to the limit imposed by Heisenberg uncertainty principle. The density distribution is shown in Fig. 1 (a).

The interaction among the exciton-polaritons generates a non-linear term in Eq. (2) and has significant effect on the condensate properties. Originated from the interaction between the exciton components, the interaction energy in our model depends on the density of the exciton-polaritons as is described in the main text. When the density n increases, the interaction energy $U(n') = gn'$ increases with density but saturates at large density. This means that the interaction constant g decreases with n' . In an inhomogeneous system, this causes a spatial dependence of the interaction energy, which introduces a second-fold non-linearity in the system besides the conventional non-linearity in the GP equation.

The finite lifetime of exciton-polaritons affects the measurement of the condensate and induces some complication for the calculation. First, only a finite time window is available for the measurement of the leakage photons. During this time window, a substantial proportion of the non-condensed exciton-polaritons exists outside the trap. Second, the diffusion time of the injected exciton-polaritons is very long compared with the condensate lifetime. As a result, the exciton polaritons outside the trap can be treated as a static background field that interacts with the condensate. We construct a simple model to describe these effects. The condensate is largely localized inside the trap. The exciton-polaritons outside the trap are treated as “idle” particles. The exciton-polaritons outside the trap, with a density of $n'_{ext} \simeq n'/2$ half of the density inside the trap due to absorption of pump photons in a metal film, are treated as an effective trapping potential.

We calculate the condensate properties for a wide range of pumping levels. In Fig. 1 (b), the spatial distribution of the condensate is shown for $P/P_{th} = 5$. Compared with the non-interacting case, the interaction flats out the density into two sections. At $r \leq R_0$ (inside the trap), the condensate has a nearly uniform density; at $r > R_0$ (outside the trap), the density quickly decreases. The low density core at $r \sim 0$ is a numerical artifact due to the chosen boundary condition.

The standard deviation of the condensate in coordinate space is calculated using a density-dependent interaction constant g . The calculated results agree well with the measurement results except for the pump rate very close to

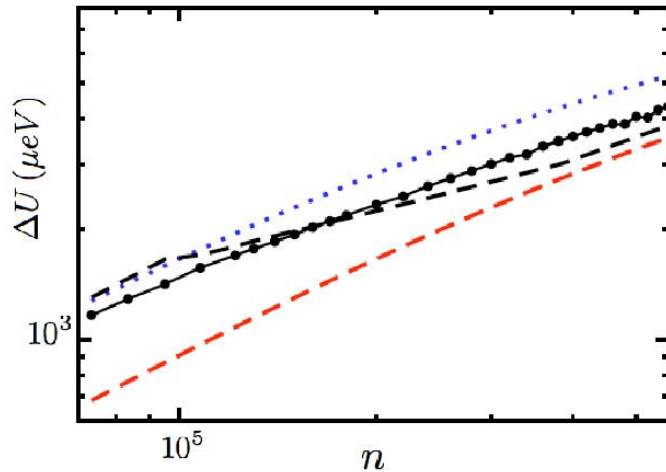


FIG. 2: Solid circle: the condensate energy per particle ε_0 versus total number of injected exciton-polaritons n inside a trap, calculated with the GP equation approach, which is shown in Fig. 1(d) in the main text by red dots. Blue dotted line: the interaction energy $U(n')$ calculated by Eq. (1) in the main text. Black dashed line: the interaction energy $U_{in} = gn'(r < R_0)$ due to the polaritons inside the trap. Red dashed line: the interaction energy $U_{ext} = gn'_{ext}$ due to the polaritons outside the trap.

condensation threshold, as is shown in Fig. 1(c) in the main text. As described in the next section, the condensation near threshold does not necessary occur at the ground state so that the observed δx is larger than the theoretical value. At high pumping level, the size increase of the condensate saturates. Here, the increasing pump power increases the spatial density of the exciton-polaritons, and hence the interaction energy $gn'(r)$, which makes the condensate expand to a larger size. However, when condensate expands too much, the interaction $gn'(r)$ decreases with the reduced density, which then acts as back action to limit the growth of the condensate. Similarly, the standard deviation in momentum space can also be calculated. The condensate wave function in momentum space is $\psi_k \propto \int r dr J_0(kr) \Psi_0(r)$ where $k = |\vec{k}|$ and $J_0(kr)$ is the zeroth order Bessel function. The results are presented in Fig. 1(c) in the main text.

The condensate energy per particle ε_0 can also be calculated with the GP equation. For a homogeneous system, ε_0 is directly connected to the interaction energy $U(n') = g(n') \cdot n'$, and the measured ε_0 can be used to analyze the properties of the ground state as well as the excitations. We numerically calculate ε_0 for the trapped system. The results are shown in Fig. 2. In our system, ε_0 includes contributions from the interaction between the condensate particles $g|\Psi_0(r)|^2$, the effective potential, and the kinetic energy due to the change of the condensate geometry. Our results show that $\varepsilon_0 \sim U_{in}$ (interaction energy inside the trap) in a wide range of the pumping levels. This is because most of the condensate particles are in the central plateau as shown in Fig. 1 (b), where we have a locally homogeneous system with the interaction U_{in} .

II. CHARACTERISTICS OF TRAPPED CONDENSATES

Figure 3 shows the momentum distributions of exciton-polaritons in a trap (diameter $d \sim 8\mu m$, $\Delta = 5.4$ meV) below and above condensation threshold that are measured in the far-field plane. The numbers at bottom right corner of each figure shows the pumping rates normalized by threshold (P/P_{th}). The momentum distribution is large and isotropic below threshold, which are the characteristics of thermal polaritons. The condensation threshold is characterized by the sudden decrease of the momentum distribution. Above threshold the momentum distribution remains almost constant, which are caused by the subtle balance between the particle-particle interaction and the

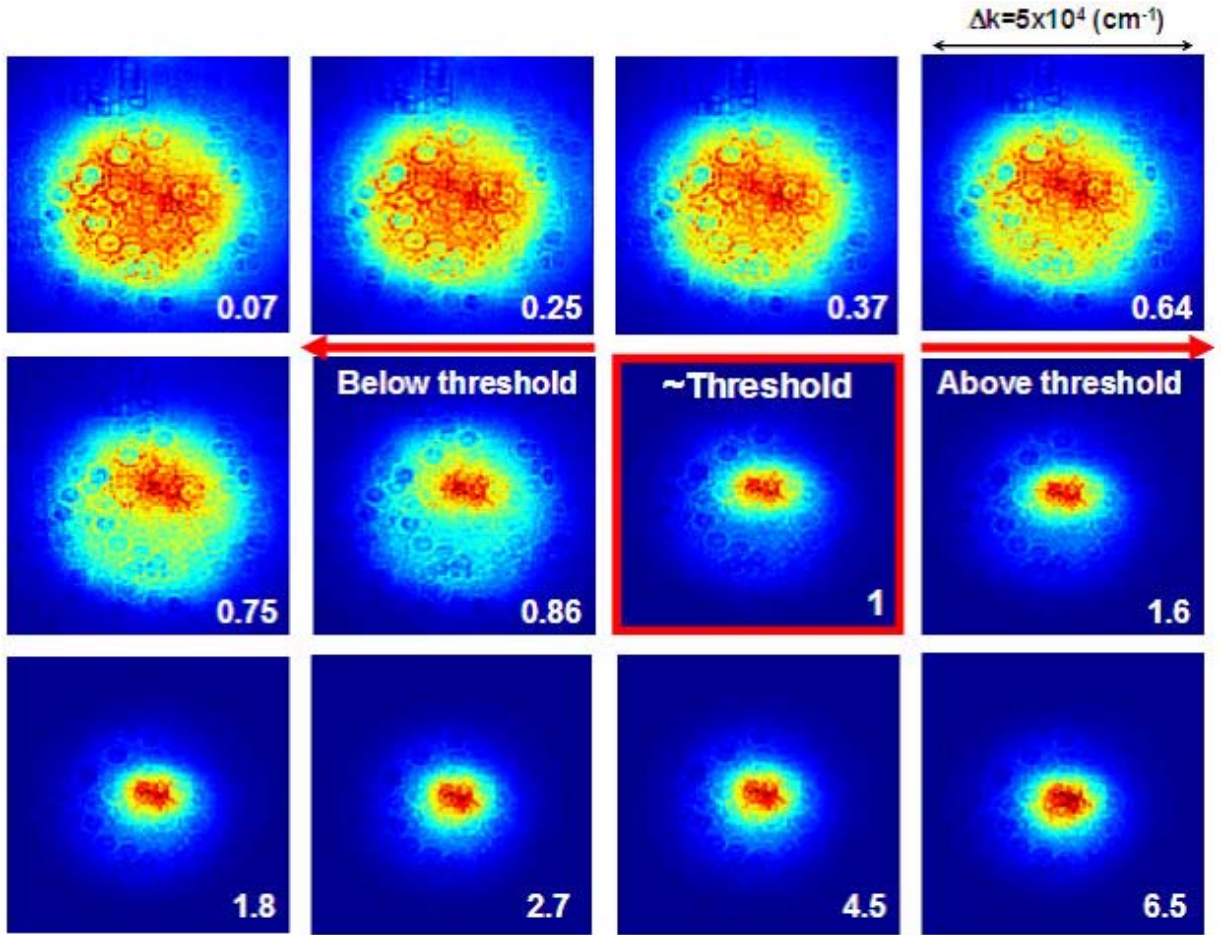


FIG. 3: Evolution of the far field pattern (momentum distribution) of exciton-polaritons in a trap for varying pump rates across condensation threshold

increased spatial distribution.

The position distributions in the same trap as Fig. 3 at pump rates below and above condensation threshold, that are measured in the near-field plane, are plotted in Fig. 4. The position distribution is isotropic and constant over varying pump rates below threshold, but suddenly decreases at threshold. The rapid increase due to polariton-polariton interaction is clearly observed above threshold. Just above threshold, the position distribution is smaller than the trap size. In this regime, the condensate is described by an inhomogeneous model rather than homogeneous model. At higher pump rates, wave function expands uniformly inside a trap and the condensate is described by a homogeneous model.

The dispersion relation (E vs. k) of exciton-polaritons in another trap (diameter $d \sim 8\mu m$, on resonance) below and above condensation threshold, measured in the far-field plane, are plotted in Fig. 5. The quadratic dispersion of excitons below threshold and linear dispersion of Bogoliubov excitons at well above threshold can be distinguished. The concentration of the polariton population into the $k = 0$ ground state and the blue shift of the ground state energy are clearly seen.

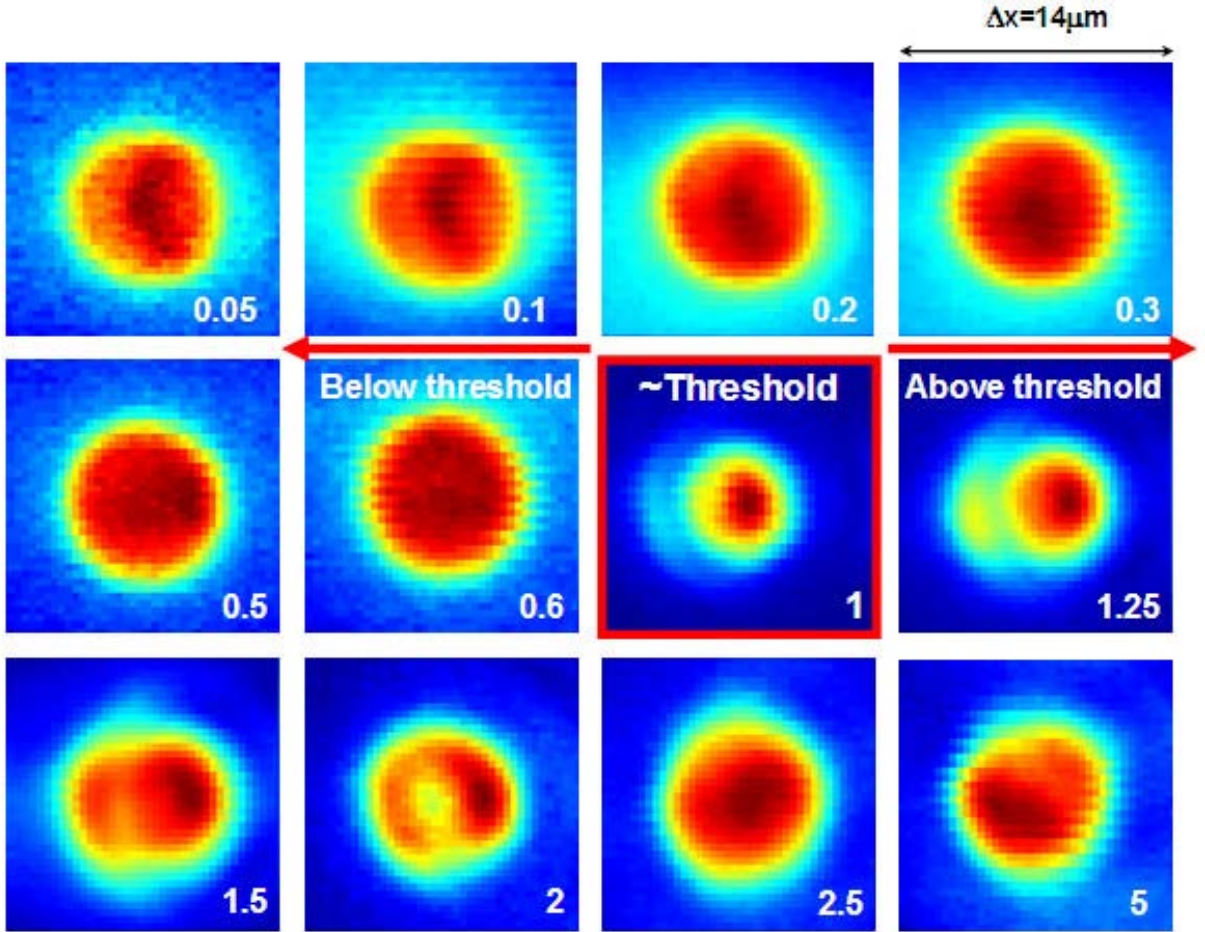


FIG. 4: Evolution of the near field pattern (position distribution) of exciton-polaritons in a trap for varying pump rates across condensation threshold

III. DYNAMIC STRUCTURE FACTOR AND EXCITATIONS

A. The solutions of the GP equation for a trapped system

We assume the exciton-polaritons satisfy the conditions of diluteness and small thermal depletion (27-33). The diluteness condition and small thermal depletion condition are given by $U \ll k_B T_c$ and $T \ll T_c$ (14), where T_c is a BEC critical temperature and T is a polariton temperature. Both conditions are satisfied at pump rates well above threshold.

The GP equation can be used to study the properties of the excitations as well as the condensate if those conditions are satisfied. Below we calculate the eigenfunctions and eigenenergies of the excitations. Assuming the excitation in the form of a small oscillation with frequency ω , we have

$$\Psi(r, t) = (\Psi_0(r) + \frac{u(r)}{\sqrt{r}} e^{il\theta} e^{-i\omega t} + \frac{v^*(r)}{\sqrt{r}} e^{-il\theta} e^{i\omega t}) e^{-i\frac{\epsilon_0}{\hbar} t}, \quad (3)$$

where $e^{il\theta}$ is the angular part of the excitation with index l . By substituting Eq. (3) into Eq. (1) and collecting terms

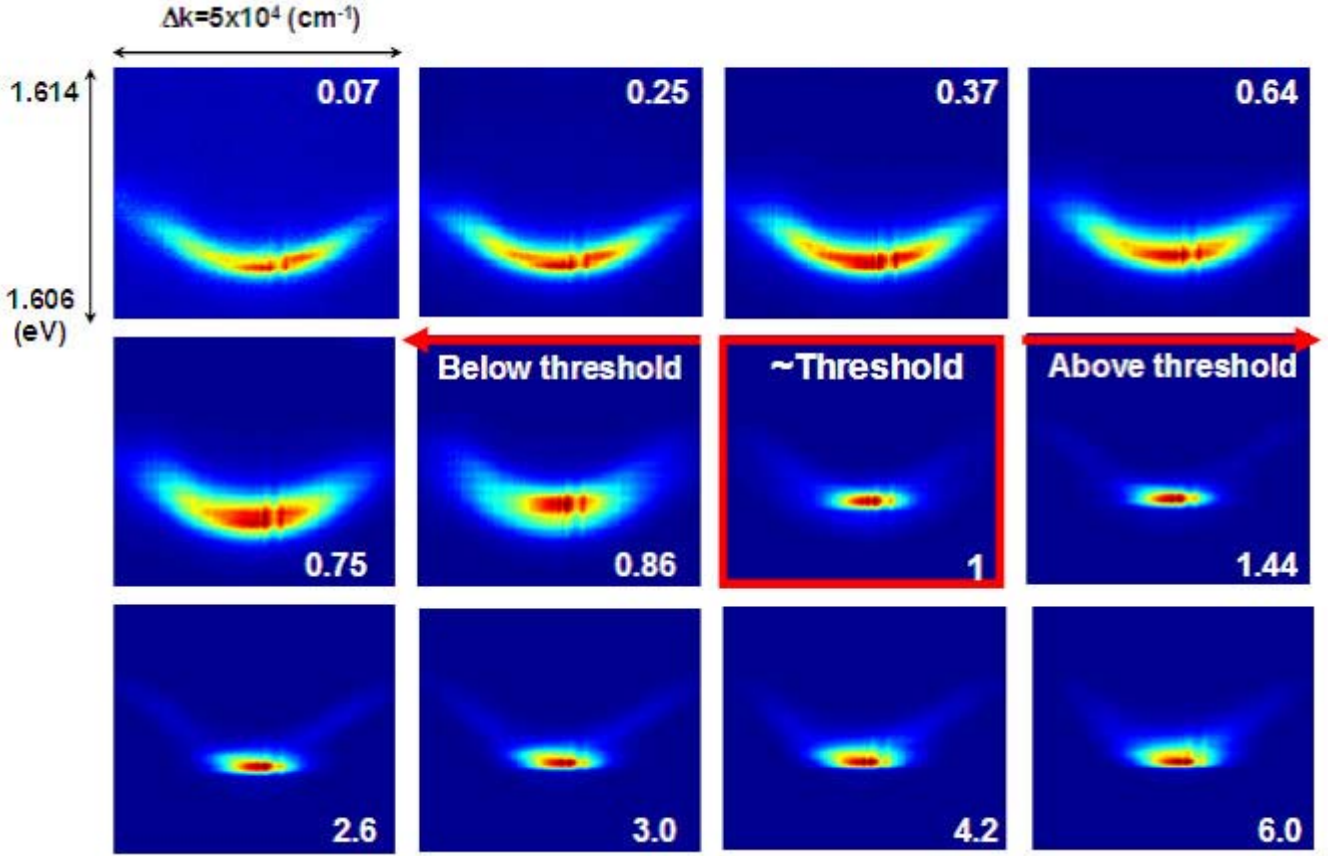


FIG. 5: Evolution of the dispersion relation (E vs. k) of exciton-polaritons in a trap for varying pump rates across condensation threshold

of $e^{\pm i\omega t}$ respectively, we obtain the following coupled equations

$$\begin{aligned} \hbar\omega u(r) &= \left\{ -\frac{\hbar^2}{2m} \left[\frac{\partial^2}{\partial^2 r} + \left(\frac{1}{4} - l^2 \right) \frac{1}{r^2} \right] + 2g \frac{\phi_0^2(r)}{r} + V(r) - \varepsilon_0 + V_{eff}(r) \right\} u(r) + g \frac{\phi_0^2(r)}{r} v(r) \\ -\hbar\omega v(r) &= \left\{ -\frac{\hbar^2}{2m} \left[\frac{\partial^2}{\partial^2 r} + \left(\frac{1}{4} - l^2 \right) \frac{1}{r^2} \right] + 2g \frac{\phi_0^2(r)}{r} + V(r) - \varepsilon_0 + V_{eff}(r) \right\} v(r) + g \frac{\phi_0^2(r)}{r} u(r) \end{aligned} \quad (4)$$

for the positive frequency component $u(r)$ and the negative frequency component $v(r)$, with the conditions $\hbar\omega > 0$ and $\int 2\pi dr (|u(r)|^2 - |v(r)|^2) = 1$. For a homogeneous system, the solution of Eq. (4) is a mixing between the plane wave modes of $e^{\pm i\vec{k}\cdot\vec{r}}$ with $u_k(\vec{r}) = e^{i\vec{k}\cdot\vec{r}} u_k$, $v_k(\vec{r}) = e^{-i\vec{k}\cdot\vec{r}} v_k$, and $\int 2\pi dr (u_k^2 - v_k^2) = 1$. The corresponding dispersion relation is the familiar form $E_k \equiv \hbar\omega_k = \sqrt{\varepsilon_k^2 + 2\varepsilon_k g n'}$ with $\varepsilon_k = \frac{(\hbar k)^2}{2m}$.

For the trapped system, the coupled equations in Eq. (4) need to be solved numerically. In Fig. 6, we plot the solutions of several excitation modes at various frequencies ω . For the low-frequency mode $\hbar\omega = 0.02 meV$, the eigenfunction of the excitation is a nearly equal mixing between the positive frequency component and the negative frequency component, indicating that the interaction $g\phi_0^2/r$ plays a significant role. For the high-frequency mode $\hbar\omega = 7.48 meV$, the kinetic energy ε_k dominates over the interaction energy, and the two components are almost decoupled with $v(r) \rightarrow 0$.

In an inhomogeneous condensate, modes with different momentum k become coupled and the plane wave solution is not the eigenmode any more. Only when $\varepsilon_k \gg g\phi_0^2/r$, the k modes become eigenmodes again. To study the property of excitations, we calculate the dynamic structure factor defined as $S(k, \omega) = \sum_{\alpha} |\langle \Phi_{\alpha} | \hat{\rho}_{\vec{k}} | \Phi_g \rangle|^2$ at zero temperature (14), where the summation is over all the many body states Φ_{α} except for the ground state and $\hat{\rho}_{\vec{k}} = \int dr e^{i\vec{k}\cdot\vec{r}} \hat{\rho}(\vec{r})$

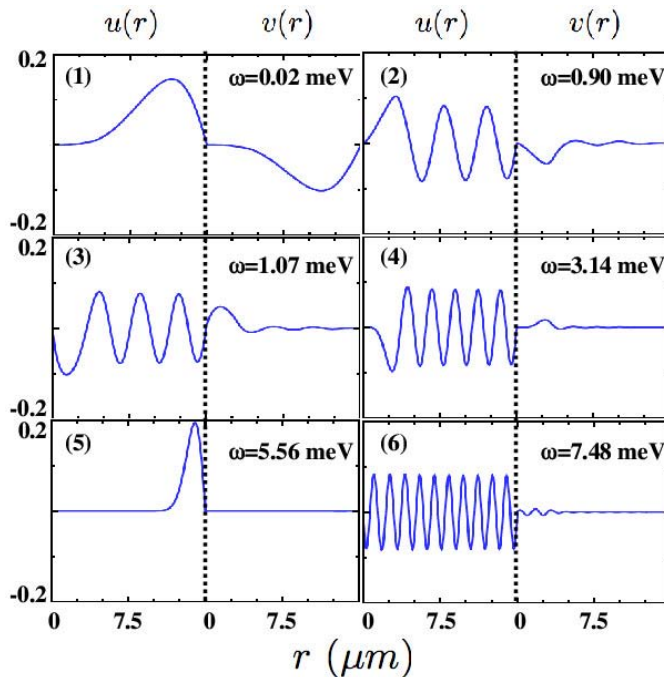


FIG. 6: Wave functions ($u(r), v(r)$) of the excitations at six different energies. The energy of each mode is labeled in the corresponding panel in the figure. In each panel, the positive frequency component $u(r)$ is plotted to the left of the dashed line and the negative frequency component $v(r)$ is plotted to the right of the dashed line. The index l in the angular component $e^{il\theta}$ of each mode is $l = 2, 1, 0, 5, 51, 0$ respectively for the six modes.

with $\rho(\vec{r})$ being the density operator. The dynamic structure factor provides information of the excitations of the condensate. It can be shown that

$$S(k, \omega) = \sum_{\alpha} \left| \int r dr d\theta (u_{\alpha}^*(r) + v_{\alpha}^*(r)) e^{-il_{\alpha}\theta} e^{ikr \cos \theta} \frac{\phi_0(r)}{r} \right|^2 \delta(\omega - \frac{\epsilon_{\alpha}}{\hbar}) \quad (5)$$

where the condensate energy ϵ_0 is taken as zero energy point, ϵ_{α} is the energy and l_{α} is the angular index of the α th excitations calculated from Eq. (4). In the numerical calculation, the δ -function is treated as

$$\delta(\omega - \omega_0) \rightarrow \frac{\delta_0}{\delta_0^2 + (\omega - \omega_0)^2}$$

with a small energy with δ_0 describing the broadening of the spectrum. In a homogeneous system, $S(k, \omega) = n\delta(\omega - \frac{\epsilon_k}{\hbar}) \frac{\epsilon_k}{\sqrt{\epsilon_k^2 + 2gn'\epsilon_k}}$ has the form of a δ -function.

In Fig.7, the calculated $S(k, \omega)$ for $P/P_{th} = 5$ is shown, where we set $\delta_0 = 0.2 meV$. At small momentum k with $|k\xi| \lesssim 0.2$, the intensity of $S(k, \omega)$ is very weak, which means that the quasiparticle population in this regime is small. In our model, the condensate ground state has a finite width of Δk in momentum space due to the finite spatial extent Δx . Hence, the excitations prefer to occupy phase space outside this regime, as can be seen in Fig. 6. Outside this regime, we can define an average dispersion relation ω_k by searching the momentum k of the maximum in $S(k, \omega)$ at fixed $\hbar\omega$. For $\epsilon_k < g\phi_0^2/r$, a linear behavior can be seen in $\hbar\omega$ vs. $k\xi$, indicating the phonon-like behavior of the excitations. For $\epsilon_k > g\phi_0^2/r$ at large k , the average dispersion approaches $\epsilon_k + \Delta$, showing the behavior of free particle, but with an energy shift of $\Delta = 0.38 meV$. This shift is much smaller than what is measured in the experiment. This difference stems from the fact that the theoretical result is the averaged interaction over the entire range of the system, while in the experiment the data were taken for the central plateau with the radii of $4 - 5 \mu m$. With a local density of $|\Psi_0(r)|^2$, the energy shift can be written as $\Delta = g|\Psi_0(r)|^2$, following the prediction of the Bogoliubov

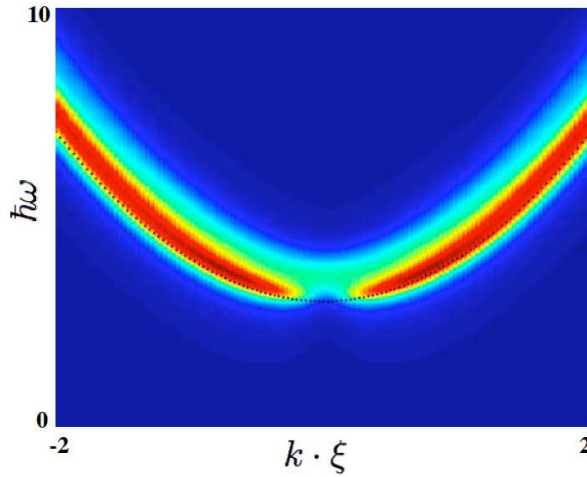


FIG. 7: $S(k, \omega)$ for $P/P_{th} = 5$ with $\xi = 0.6 \mu m$ and the unit for $\hbar\omega$ is meV . The dotted line is the free particle dispersion starting from the condensate energy.

theory. In our trapped system, the density can be approximated as $\sim |\Psi_0(r)(r = 2.5 \mu m)|^2$ and the interaction constant is $g = 8.9 \times 10^{-38}$ in unit of $J \cdot m^2$, we have $\Delta = 1.12 meV$ which agrees with the experimental energy shift.

B. The solutions of the GP equation for an untrapped system

The above estimation is based on the so called local density approximation (LDA). In the following, we apply the LDA method to study the untrapped condensate. We assume that the density of the system varies smoothly over the space with the density $n'(r)$. The dynamic structure factor under the LDA can be written as

$$S_{LDA}(k, \omega) = \int 2\pi r dr n'(r) \delta(\omega - \omega_k) \frac{\epsilon_k}{\hbar\omega_k}$$

where $\hbar\omega_k = \sqrt{\epsilon_k^2 + 2\epsilon_k g n'(r)}$. The n th order moment of the structure factor is $M_n(k) = \int_0^\infty d\omega \omega^n S(k, \omega)$. The average excitation energy at momentum q can be derived as $\bar{\omega}(k) = \hbar M_1(k)/M_0(k)$.

We consider a Gaussian profile for the pumping laser beam. The exciton-polariton density is $n'(r) = n'_0 \exp(-r^2/\sigma)$ with n'_0 proportional to the pumping power and $\sqrt{\sigma/2}$ being the variance of the Gaussian profile. For simplicity, we assume that when $n'(r) > n'_{th}$ (n'_{th} condensation threshold), the condensate appears within the area of $r \leq R_0 = \sqrt{\sigma \log(n'_0/n'_{th})}$. For $r > R_0$, there are only free particles with $\hbar\omega_k = \epsilon_k$.

It can be derived that the first moment of the dynamic structure factor is $\hbar M_1 = n'_0 \sigma \pi \epsilon_k$ and the zeroth moment is

$$M_0 = n'_0 \sigma \pi \left\{ e^{-\frac{R_0^2}{\sigma}} + \frac{\epsilon_k}{g n'_0} \left(\sqrt{1 + \frac{2g n'_0}{\epsilon_k}} - \sqrt{1 + \frac{2g n'_0}{\epsilon_k} e^{-\frac{R_0^2}{\sigma}}} \right) \right\}. \quad (6)$$

At small ϵ_k , we can expand the expression of M_0 and derive the average energy as

$$\hbar\bar{\omega}_k = \frac{\epsilon_k}{\sqrt{\frac{2\epsilon_k}{g n'_0} (1 - e^{-\frac{R_0^2}{2\sigma}}) + e^{-\frac{R_0^2}{\sigma}}}}, \quad (7)$$

which recovers the linear dispersion of the Bogoliubov excitations when $\exp(-R_0^2/\sigma) \rightarrow 0$. At large ϵ_k , we derive the average energy as

$$\hbar\bar{\omega}_k = \epsilon_k + \varepsilon_0 \left(1 - \left(\frac{P_{th}}{P} \right)^2 \right). \quad (8)$$

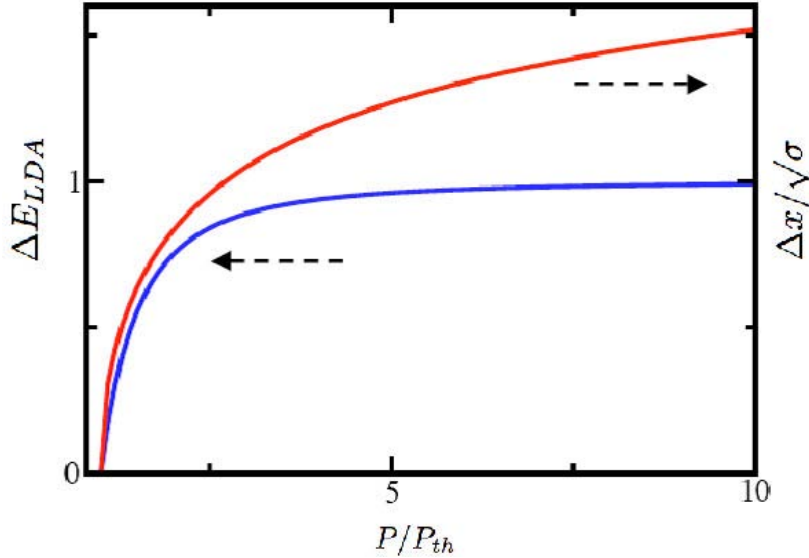


FIG. 8: Blue line: $\Delta E_{LDA} = (\hbar\bar{\omega}_k - \epsilon_k)/\epsilon_0$ and red line: $\Delta x/\sqrt{\sigma}$ with LDA method versus the pumping level.

The normalized excitation energy $\Delta E_{LDA} = (\hbar\bar{\omega}(k) - \epsilon_k)/\epsilon_0$ is plotted in Fig. 8. Note that $n'_0/n'_{th} = P/P_{th}$. It is interesting to note that $\hbar\bar{\omega}(k) - \epsilon_k$ in Eq. (8) has the same expression as the averaged condensate energy in the LDA method. Here, the averaged condensate energy is $\langle \epsilon_0 \rangle = \int 2\pi r dr n'(r) g |\Psi_0(r)|^2$. This result agrees with the experimental results shown in Fig. 4(b) and (c) in the main text.

One interesting point to note is the phonon velocity at large pumping power. Here, we have $\langle \epsilon_0 \rangle = \bar{U} = \frac{gn'_0}{2}$. From Eq. (7), the phonon velocity in the LDA method is $\bar{c} = \sqrt{\frac{\bar{U}}{2m}} \approx 0.7\sqrt{\frac{\bar{U}}{m}}$, which is in coincidence with the result for harmonically trapped condensates [14].

IV. THERMAL DEPLETION VS. QUANTUM DEPLETION

The thermodynamic behaviour of the excitations (Bogoliubov quasi-particles) can be obtained by setting the energy of the excitations, $E_k = \left[\frac{U}{m}(\hbar k)^2 + \frac{(\hbar k)^4}{4m^2} \right]^{\frac{1}{2}}$. The average occupation number of Bogoliubov quasi-particles with wavenumber k is given by

$$\langle \hat{b}_k^+ \hat{b}_k \rangle = \frac{1}{\exp(\beta E_k) - 1}. \quad (9)$$

Even though Bogoliubov quasi-particles are the convenient theoretical concept, the experimentally accessible real particles in our experiment are the lower polaritons which have a one-to-one correspondence to the energy and the momentum of the photon leaking from the cavity. Using the Bogoliubov transformation,

$$\hat{a}_k = u_k \hat{b}_k + v_{-k}^* \hat{b}_{-k}^+, \quad \hat{a}_k^+ = u_k^* \hat{b}_k^+ + v_{-k} \hat{b}_{-k}, \quad (10)$$

$$u_k, v_{-k} = \pm \left[\frac{(\hbar k)^2/2m + U}{2E_k} \pm \frac{1}{2} \right]^{\frac{1}{2}} \quad (11)$$

The real particle occupation number is given by

$$n_k \equiv \langle \hat{a}_k^+ \hat{a}_k \rangle = |u_k|^2 \langle \hat{b}_k^+ \hat{b}_k \rangle + |v_{-k}|^2 [1 + \langle \hat{b}_k^+ \hat{b}_k \rangle] \quad (12)$$

$$= |v_{-k}|^2 + \frac{|u_k|^2 + |v_{-k}|^2}{\exp(\beta E_k) - 1} \quad (13)$$

The interactions in the gas cause the presence of particles with finite k , even at absolute zero temperature where $\langle \hat{b}_k^\dagger \hat{b}_k \rangle = 0$. This is called quantum depletion and described by the first term in the right-hand side of Eq. (13). The second term in the right-hand side of Eq. (13) represents the presence of particles at finite k due to thermal excitations at finite temperatures. We can distinguish the origin of the observed Bogoliubov excitations, whether the quantum depletion or thermal depletion is responsible for the production of real particles, by examining the wavenumber dependence of the real particle population. Using Eq. (11) for v_{-k} we find the real particle occupation number at $T = 0$ and at small wavenumber $|k\xi| < 1$

$$n_k \cong \frac{1}{2\sqrt{2}|k\xi|} \quad (14)$$

where ξ is the healing length (14). n_k decreases with $\frac{1}{k}$ dependence if the quantum depletion is dominant. As pointed out already in the previous section, Eq. (14) is valid in a k region larger than the momentum uncertainty Δk of the condensate.

Next, let us consider the thermal depletion. In the low energy regime where $E_k \ll k_B T$. Eq. (9) is reduced to $\langle \hat{b}_k^\dagger \hat{b}_k \rangle \cong k_B T / E_k$. From Eq.(11) for u_k and v_{-k} , we find, at small wavenumber $|k\xi| < 1$, $|u_k|^2 + |v_{-k}|^2 = \frac{U}{E_k}$. Using the relations in the second term of the right-hand side of Eq. (13), the real particle occupation number at finite temperatures is given by

$$n_k \cong \frac{mk_B T}{(\hbar k)^2} \quad (15)$$

n_k decreases with $\frac{1}{k^2}$ dependence if the thermal depletion is dominant.

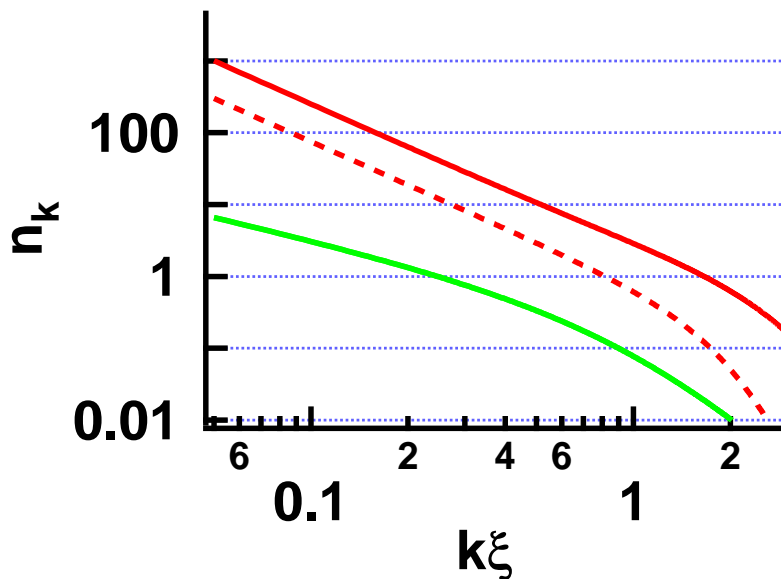


FIG. 9: **Real particle (lower polariton) number n_k vs. normalized wavenumber.** Red solid line shows the real particle (lower polariton) number n_k using an effective temperature and polariton-polariton interaction energy as $k_B T = 10$ meV and $U = 2$ meV, respectively. Red dotted line shows n_k for $k_B T = 3$ meV and $U = 2$ meV. The component of quantum depletion $|v_{-k}|^2$ is plotted as green solid line for $U = 2$ meV, which are degenerate for the above two cases.

Figure 9 shows the real particle (lower polariton) number n_k vs. the normalized wavenumber $k\xi$ using Eq. (13) for the typical experimental parameters in our system. In the exciton-polariton condensate, temperature T is a

dynamical variable as a function of time after impulsive injection of high-energy exciton-polaritons (13). The time resolved measurement of lower polariton population distribution $n_k(t)$ allows us to determine the time-dependent gas temperature $T(t)$. (Fig. 3 in (13)). By integrating those variables weighted by the emission intensity, we will obtain the time averaged temperature of the polariton gas. The averaged polariton temperature $k_B T$ ranges from 3-10 meV, depending on the detuning parameter and the pump rate. If we use those parameters with the observed interaction energy $U \simeq 2$ meV, we confirm the thermal depletion is indeed dominant over the quantum depletion in our experimental system, as shown in Fig. 9. The thermal depletion dominates over the quantum depletion by one to two orders of magnitude in the experimental systems. The experimental results shown in Fig. 4(d) in the main text show the $\frac{1}{k^2}$ dependence, which suggests the Bogoliubov excitations are produced by the thermal depletion in our experiment.

Bibliography

- [27] Lee, T. D., Huang K. and Yang, C. N. Phys. Rev. 106, 1135-1145 (1957)
 - [28] Lee, T. D. and Yang, C. N. Phys. Rev. 105, 1119-1120 (1957).
 - [29] Nozieres, P. and Pines, D. The theory of quantum liquids (Perseus Books, Cambridge, Mass., 1999).
 - [30] Landau, L. D., Pitaevskii, L. P. and Lifshits, E. M. Statistical physics, Part 2 (Pergamon Press, Oxford ; New York, 1980).
 - [31] Leggett, A. J. Quantum liquids: Bose condensation and Cooper pairing in condensedmatter systems (Oxford University Press, Oxford ; New York, 2006).
 - [32] Leggett, A. J. Rev. Mod. Phys. 73, 307-356 (2001).
 - [33] Hora, C. and Castin, Y. Phys. Rev. A 67, 053615 (2003)
-